Article

Topological complex-energy braiding of non-Hermitian bands

https://doi.org/10.1038/s41586-021-03848-x

Received: 26 February 2021

Accepted: 21 July 2021

Published online: 6 October 2021

Check for updates

Kai Wang[1], Avik Dutt[1], Charles C. Wojcik[1] & Shanhui Fan[1]✉

Effects connected with the mathematical theory of knots[1] emerge in many areas of science, from physics[2,3] to biology[4]. Recent theoretical work discovered that the braid group characterizes the topology of non-Hermitian periodic systems[5], where the complex band energies can braid in momentum space. However, such braids of complex-energy bands have not been realized or controlled experimentally. Here, we introduce a tight-binding lattice model that can achieve arbitrary elements in the braid group of two strands $\mathbb{B}_2$. We experimentally demonstrate such topological complex-energy braiding of non-Hermitian bands in a synthetic dimension[6,7]. Our experiments utilize frequency modes in two coupled ring resonators, one of which undergoes simultaneous phase and amplitude modulation. We observe a wide variety of two-band braiding structures that constitute representative instances of links and knots, including the unlink, the unknot, the Hopf link and the trefoil. We also show that the handedness of braids can be changed. Our results provide a direct demonstration of the braid-group characterization of non-Hermitian topology and open a pathway for designing and realizing topologically robust phases in open classical and quantum systems.

There are deep connections between the mathematics of knots and fundamental physics. Knots exhibit a highly complex set of topological invariants[8]. Therefore, a physical field with knot configurations is endowed with a rich and diverse class of topologically stable behaviours. This observation has long motivated efforts to explore the physical consequences of the topology associated with knots, from Lord Kelvin's vortex atom hypothesis more than 100 years ago[9] to recent research in areas such as photonics[2,3,10,11], condensed matter physics[12–15] and high-energy physics[16].

Very recently, it was noted that the energy bands of one-dimensional non-Hermitian systems form braids, which are intimately related to knots[8], and the conjugacy classes of the braid groups classify the topology of such bands[5,17]. Non-Hermitian theory describes open systems such as photonic structures with gain and/or loss[18–23], or quasi-particles with finite lifetimes in condensed matter[24,25]. Developing an understanding of the topology of energy bands in non-Hermitian systems is vital in creating open quantum and classical systems that are topologically robust. The braid-group classification highlights unique aspects of band structures induced by non-Hermiticity[5,17,26]. Moreover, the highly intricate nature of the braid groups indicates significant potential for exploring and exploiting a large number of distinct topological effects in non-Hermitian systems.

As an important step towards realizing such potentials, we introduce an approach to construct non-Hermitian models that can achieve the entire two-strand braid group $\mathbb{B}_2$. Using this approach, we provide the first experimental observation of non-Hermitian energy band structures exhibiting non-trivial knots and links. Our experimental demonstration makes use of the concept of synthetic dimensions[6,7,27,28], as we implement several non-Hermitian lattice Hamiltonians in a frequency synthetic dimension[23,29–36] using two coupled optical ring resonators, with one undergoing simultaneous phase and amplitude modulations.

A fundamentally distinct feature of non-Hermitian systems is their complex-valued eigenenergies. For one-dimensional periodic non-Hermitian Hamiltonians, as the momentum k is restricted to the first Brillouin zone $(0, 2\pi)$, each energy band, as described by a momentum (k)-dependent complex energy $E(k)$, can be regarded as a strand of a braid in the $(\mathrm{Re}(E), \mathrm{Im}(E), k)$-space (this three-dimensional space is denoted as the E–k space below)[5,17]. Moreover, as the momenta at the two ends of the Brillioiuin zone are equivalent, the two ends of the braids can be identified, which closes the braids to form knots or links. Thus, in general, one-dimensional non-Hermitian band structures can be described by knots or links. Achieving topologically different band structures then corresponds to creating different knots or links in the E–k space.

To obtain a specific knot or link by closing a braid, there exists a minimum necessary number of strands in the braid, known as the braid index[8]. Given that all knots and links other than the unknot have a braid index larger than one, a single band can only form an unknot (see Supplementary Information, section 1B, for details). Thereby, the topology associated with a single band is limited. The topological invariant of a single band has to be defined in regard to the winding around a reference energy[23,37,38]. By contrast, the topological invariants of N bands are the braid group $\mathbb{B}_N$, which is defined without the need of a reference energy, and becomes non-trivial for $N > 1$ (ref. [5]).

Specific theoretical models that can realize limited numbers of two-band complex-energy braiding have been proposed[39,40]. Here, we experimentally demonstrate a tight-binding lattice model that can realize arbitrary times of braiding with two energy bands. The Hamiltonian we construct is in the form:

[1]Ginzton Laboratory and Department of Electrical Engineering, Stanford University, Stanford, CA, USA. ✉e-mail: shanhui@stanford.edu

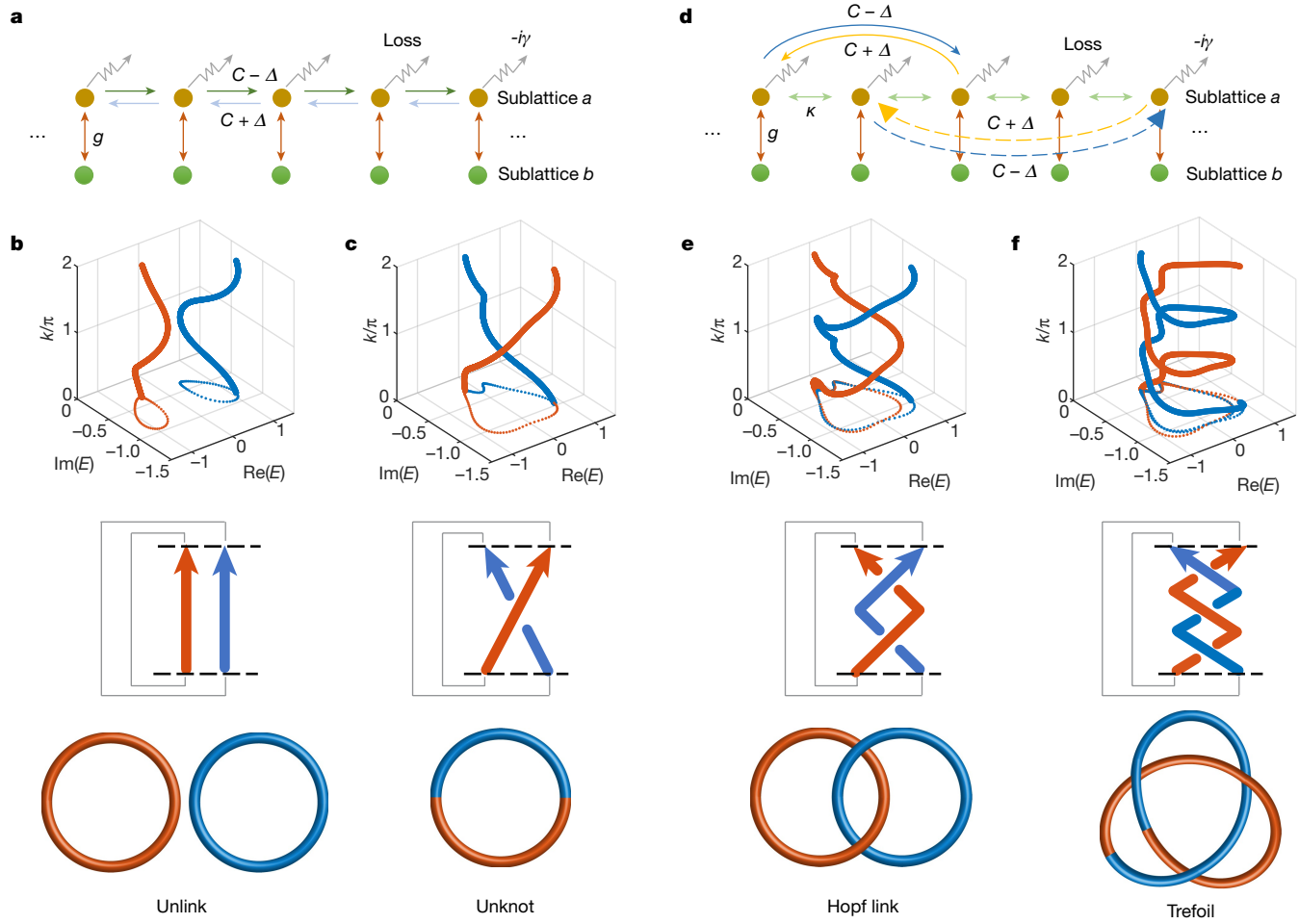

Fig. 1 | Braiding of two non-Hermitian bands. a, Sketch of two-band lattice model with $m = 1$. **b**,**c**, Top, two examples of complex band-energy braiding in the (Re(E), Im(E), k)-space for the lattice model in **a** with a specific choice of parameters, and the dotted curves are projections of the bands in the $k = 0$ plane. Middle, corresponding braid diagrams with braid closures by the grey lines. Bottom, corresponding knot diagrams. **d**, Sketch of two-band lattice model with $m = 2$ (curved solid arrows show second-order coupling) and $m = 3$ (curved dashed arrows show third-order coupling). **e**,**f**, Same as **b**,**c**, but for the model sketched in **d** in the cases of $m = 2$ (**e**) and $m = 3$ (**f**) for specific choices of parameters.

$$\mathbf{H}^{(m)} = \sum_n g\mathbf{a}_n^\dagger \mathbf{b}_n + g\mathbf{b}_n^\dagger \mathbf{a}_n - i\gamma \mathbf{a}_n^\dagger \mathbf{a}_n + \kappa \mathbf{a}_{n+1}^\dagger \mathbf{a}_n + \kappa \mathbf{a}_n^\dagger \mathbf{a}_{n+1} + (C-\Delta)\mathbf{a}_{n+m}^\dagger \mathbf{a}_n + (C+\Delta)\mathbf{a}_n^\dagger \mathbf{a}_{n+m}, \quad (1)$$

where $\mathbf{a}_n^\dagger$ ($\mathbf{a}_n$) and $\mathbf{b}_n^\dagger$ ($\mathbf{b}_n$) denote the creation (annihilation) operators of the n-th lattice site in sublattices a and b, respectively. The parameters $\kappa, g, C \pm \Delta \in \mathbb{R}$ denote coupling constants, and $\gamma > 0$ represents the additional loss rate in sublattice a in excess of the loss rate in sublattice b (we note that a globally uniform loss rate does not affect the topology of the bands and is omitted from equation (1)). Such a model has nearest-neighbour coupling as well as coupling between the m-th neighbours within sublattice a. Each lattice site on sublattice a in addition couples to a site on sublattice b. There is no coupling between the sites on sublattice b (Fig. 1a,d). With a judicious choice of parameters, energy bands $E_\pm(k)$ for the Hamiltonian of equation (1) can satisfy the separable band condition[40] (that is, $E_+(k) \neq E_-(k)$ for all k). The topology of two such separable energy bands is classified by the braid group $\mathbb{B}_2$. To determine the element in $\mathbb{B}_2$ associated with a specific two-band model, as $\mathbb{B}_2$ is isomorphic to the group of integers $\mathbb{Z}$, we define an integer topological invariant, namely the degree of a two-strand braid,

$$\upsilon := \int_0^{2\pi} \frac{\mathrm{d}k}{2\pi i} \frac{\mathrm{d}}{\mathrm{d}k} \ln \mathrm{Det}\left[\mathbf{H}_k^{(m)} - \frac{1}{2}\mathrm{Tr}\left(\mathbf{H}_k^{(m)}\right)\right], \quad (2)$$

where $\mathbf{H}_k^{(m)}$ is the k-space representation of the Hamiltonian $\mathbf{H}^{(m)}$ in equation (1). This braid degree describes how many times the two bands braid in the E–k space as k varies from 0 to 2π, with the sign of υ indicating the handedness of the braid. Different from the winding numbers defined in the point-gap topology for non-Hermitian Hamiltonians[37,38,41], the braid degree given in equation (2) does not involve any choice of reference energy. This topological invariant is closely related to the vorticity defined for separable bands[40].

To understand the behaviour of the Hamiltonian in equation (1), we start with a simple example in which we sketch the lattice model having $m = 1$ (Fig. 1a). In this case, within sublattice a there is only nearest-neighbour coupling. Hence, without loss of generality we can take $\kappa = 0$, and the couplings within sublattice a are $C \pm \Delta$. The k-space Hamiltonian in this case can be written into a 2×2 matrix form,

$$\mathbf{H}_k^{(1)} = \begin{bmatrix} 2C\cos k + i2\Delta \sin k - i\gamma & g \\ g & 0 \end{bmatrix}, \quad (3)$$

with the k-dependent band energies given by

$$E_\pm^{(1)}(k) = C\cos k + i\Delta \sin k - i\frac{\gamma}{2} \pm \sqrt{\left(C\cos k + i\Delta \sin k - i\frac{\gamma}{2}\right)^2 + g^2}. \quad (4)$$

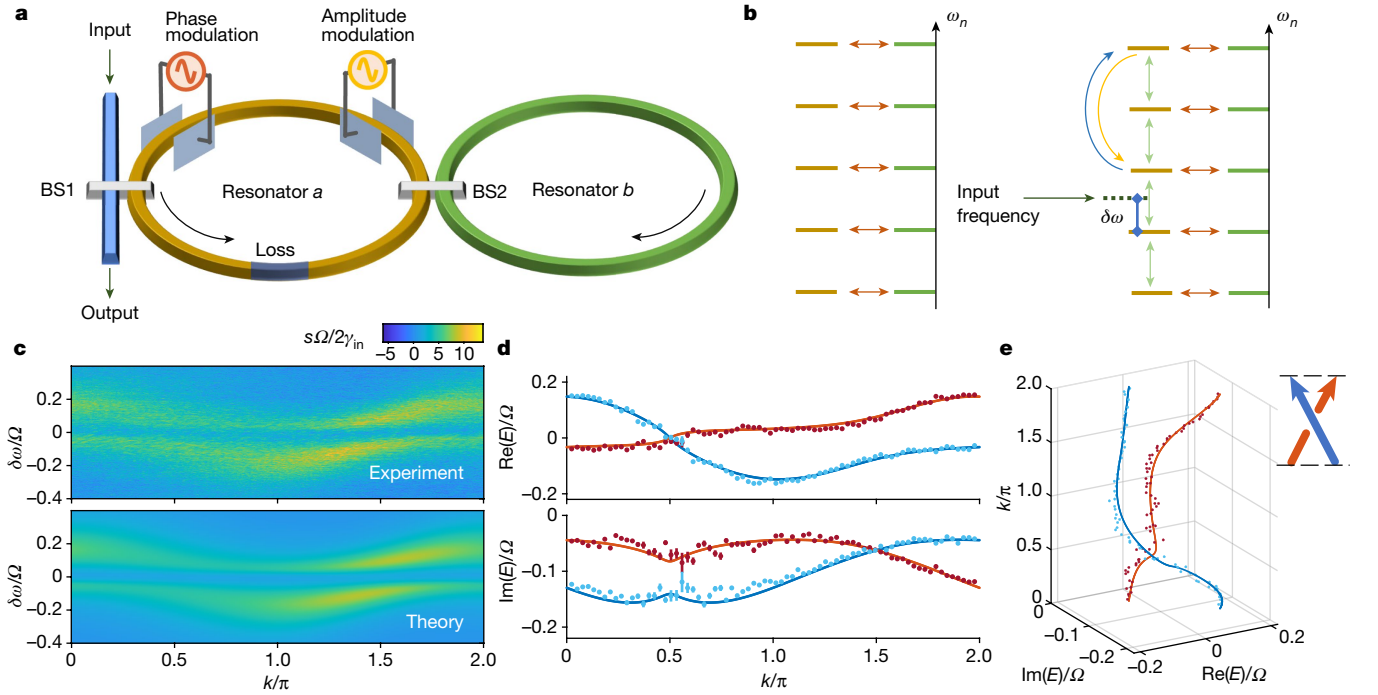

Fig. 2 | Realization of two-band complex-energy braids in a frequency synthetic dimension. a, Conceptual sketch of the experimental realization using frequency modes in two coupled ring resonators. **b**, Discrete frequencies in the two resonators (left) in the absence of modulation and (right) in the presence of an example modulation. The input laser frequency $\omega = \omega_n + \delta\omega$ is detuned by $\delta\omega$ from a certain resonance frequency ω_n. **c**, An example of a transmission signal $s(k, \delta\omega)$ versus $\delta\omega$ and k measured in the experiment (top) and the corresponding theoretical predictions (bottom). **d**, Extracted real and imaginary band energies from **c** (top), where dots denote experimental data and curves are theoretical predictions. Error bars represent 95% confidence intervals in the data extraction based on fitting. **e**, Plot of the complex bands of **d** in the E–k space, accompanied by the corresponding braid diagram.

Depending on the choice of parameters, the two band energies can either braid into two separate loops (Fig. 1b) or one loop (Fig. 1c). In the example shown (Fig. 1b, top), we take $\Delta = 0.15$, $C/\Delta = 2.1$, $\gamma/\Delta = 8$, $g/\Delta = 6$. The two complex-energy bands (denoted by strands with different colours) do not braid around each other. This case can be represented by a braid diagram (as shown in Fig. 1b, middle); the braid degree $\upsilon = 0$. The identification of the ends of each strands at $k = 0$ and $k = 2\pi$ results in two separate loops, or an unlink (as shown in Fig. 1b, bottom). By contrast, changing g/Δ to 4.3 while keeping the other parameters fixed yields a system with two bands that braid around each other after a 2π variation of k with the braid degree $\upsilon = 1$ (Fig. 1c, top). This braid can be represented by the length-one braid word σ (Fig. 1c, middle)), where σ is a transposition generating the two-strand braid group $\mathbb{B}_2$. The resulting knot is a single loop, which corresponds to an unknot (Fig. 1c, bottom).

To obtain more complex braids with $|\upsilon| > 1$ that correspond to more complex knots and links, we use long-range couplings as described by $m > 1$ in equation (1) (Fig. 1d). In Fig. 1e we show an example with the Hamiltonian $\mathbf{H}^{(m=2)}$ taking the parameters $\Delta = 0.15$, $\kappa/\Delta = 0.04$, $C/\Delta = 2.1$, $\gamma/\Delta = 8$, $g/\Delta = 4.3$. The two bands braid around each other twice as k varies from 0 to 2π (Fig. 1e, top), hence the braid degree $\upsilon = 2$. The resulting braid is described by the braid word σ^2 (Fig. 1e, middle), which corresponds to a Hopf link (Fig. 1e, bottom). In Fig. 1f we show an example with the Hamiltonian $\mathbf{H}^{(m=3)}$ having the parameters $\Delta = -0.15$, $\kappa/\Delta = -0.04$, $C/\Delta = -2.1$, $\gamma/\Delta = -8$, $g/\Delta = -4.3$, where the braid degree $\upsilon = -3$ and the braid word becomes σ^{-3}, forming a non-trivial knot called the trefoil. In general, with a judicious choice of parameters, the Hamiltonian $\mathbf{H}^{(m)}$ in equation (1) can realize a braid with a braid word σ^m or σ^{-m} (see Supplementary Information, section 1A, for further details). This Hamiltonian can therefore realize the entire two-strand braid group $\mathbb{B}_2$. Here, the signs in the exponent of the braid words denote either a right-handed or a left-handed braid. When m is even, such a braid corresponds to a link, which consists of two disconnected loops. When m is odd, such a braid corresponds to a knot that is a single connected loop.

We now experimentally demonstrate the lattice model given in equation (1) in a frequency synthetic dimension. In Fig. 2a we show a schematic of the experimental setup that involves two fibre optical ring resonators (a and b) having the same free spectral range Ω. We use the frequency modes in the two resonators in the absence of modulation to represent the lattice sites in the model of equation (1) (Fig. 2b, left). Resonator a contains a phase and an amplitude electro-optic modulator to implement the couplings among lattice sites in sublattice a; resonator b is not modulated. The coupling between the two resonators is mediated by a fibre beam splitter (BS2). Continuous-wave laser light is injected into resonator a via another beam splitter (BS1 of Fig. 2a), with a tunable detuning $\delta\omega$ with respect to a resonance frequency ω_n (Fig. 2b, right). To extract the complex band structure, we measure a time- and detuning-dependent transmission signal $s(k, \delta\omega)$ from the output port shown in Fig. 2a, where k is essentially time. For more experimental details, see Methods and Supplementary Information, section 2.

As an illustrative example (Fig. 2c, top), we show one representative $s(k, \delta\omega)$ obtained in an experimental measurement implementing the lattice model shown in Fig. 1a with the parameters $C = 0.058\,\Omega$, $\Delta = -0.025\,\Omega$, $g = 0.087\,\Omega$, and $\gamma = 0.134\,\Omega$. The theoretically predicted $s(k, \delta\omega)$ for such parameters are also plotted (Fig. 2c, bottom). For this example, the deduced band energies are shown as dots (Fig. 2d), and these agree with theoretical predictions (curves). In Fig. 2e, we plot these data in the E–k space, accompanied by a corresponding braid diagram with the braid word σ^{-1}. The two bands braid around each other once with a left handedness, and $\upsilon = -1$.

The two-band braids we have implemented are related to the topology of Riemann surfaces in the vicinity of an exceptional point. Generalizing the k-space Hamiltonian $\mathbf{H}_k^{(1)} = (2C\cos k + i2\Delta\sin k - i\gamma)(\sigma_z + \mathbf{I}_2)/2 + g\sigma_x$ of equation (3), we can define $\mathbf{H}^{(1)}(\alpha, \beta) = (2C\alpha + i2\Delta\beta - i\gamma)(\sigma_z + \mathbf{I}_2)/2 + g\sigma_x$,

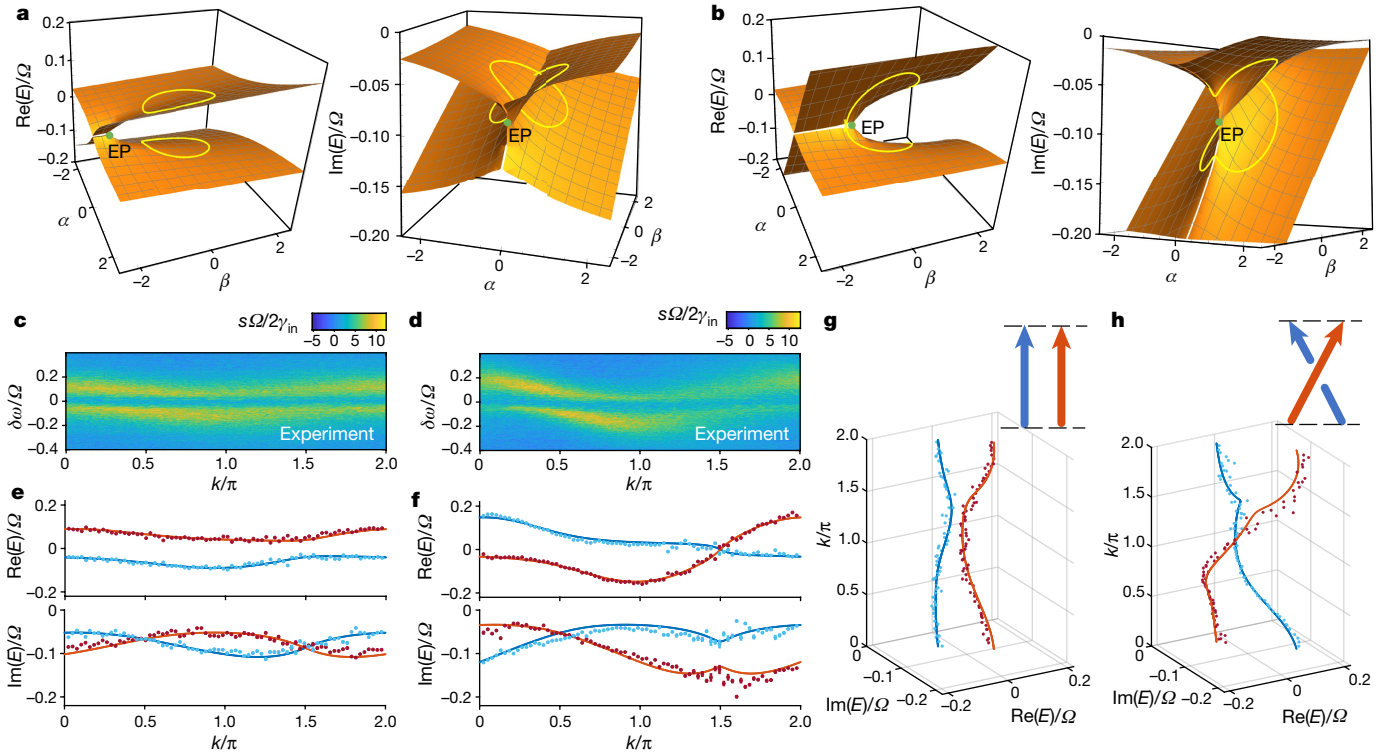

Fig. 3 | Braided non-Hermitian bands in relation to loops on Riemann surfaces. a,**b**, Band-energy trajectories (yellow curves) on a Riemann surface in the vicinity of an exceptional point (EP) P_- that (**a**) do not enclose the EP and (**b**) encircle the EP as k varies from 0 to 2π. **c**,**d**, The measured transmission signals $s(k, \delta\omega)$ for the cases shown in **a**,**b**, respectively. **e**,**f**, Extracted real and imaginary band energies from **c**,**d**, respectively, where dots denote experimental data and curves are theoretical predictions. Error bars correspond to 95% confidence intervals in the data extraction based on fitting. **g**,**h**, E–k-space plots of data in **e**,**f**, respectively, accompanied by the corresponding braid diagrams. As in **e**,**f**, dots denote experimental data and curves are theoretical predictions.

where the first Brillouin zone corresponds to a unit circle $\alpha^2 + \beta^2 = 1$ in the (α, β) space. Here, σ_x and σ_z are Pauli matrices. The eigenvalues of $\mathbf{H}^{(1)}(\alpha, \beta)$ (that is, $E_+(\alpha, \beta)$ and $E_-(\alpha, \beta)$) define two Riemann sheets of the map from the (α, β)-plane to the complex E-plane. $\mathbf{H}^{(1)}(\alpha, \beta)$ exhibits two exceptional points at $P_\pm = (0, \gamma/2\Delta \pm g/\Delta)$. The non-trivial braiding of the two bands $E_+(k)$ and $E_-(k)$ is closely related to the enclosure of an exceptional point of $\mathbf{H}^{(1)}(\alpha, \beta)$ by the unit circle. As one example, if the model in Fig. 1a with $m = 1$ takes the parameters $C = 0.024\ \Omega$, $\Delta = 0.010\ \Omega$, $g = 0.087\ \Omega$, $\gamma = 0.134\ \Omega$, the $E_\pm(\alpha, \beta)$ trajectories on the Riemann surface with (α, β) on the unit circle are shown in Fig. 3a as yellow curves. In this case, both exceptional points at $P_+ = (0, 15.4)$ and $P_- = (0, -2)$ are outside the loop, and hence the two bands do not braid, as can be seen in the measurement of the experimentally realized Hamiltonian in Fig. 3c,e,g. The braid degree $\nu = 0$, and closing the braid forms an unlink. By contrast, by changing the values of C and Δ to $C = 0.058\ \Omega$, $\Delta = 0.025\ \Omega$ (as shown in Fig. 3b), one of the exceptional points is moved inside the loop, at $P_- = (0, -0.8)$. The measured complex band structure exhibits a non-trivial braid (Fig. 3d,f,h), with a braid degree $\nu = 1$. Closing the braid forms an unknot. Here the non-trivial braid arises, as moving along a circle around an exceptional point results in the exchange of the eigenvalues of the 2×2 matrix $\mathbf{H}^{(1)}(\alpha, \beta)$. Note that the case shown in Fig. 3d,f,h has similar parameters as those used in Fig. 2c,d,e, except for a sign difference in Δ. The sign difference leads to a difference in the handedness of the braids.

Now we present experimental examples with observed braids that form a non-trivial link and knot. We experimentally realize the lattice model as sketched in Fig. 1d for $m = 2$ with the parameters $\kappa = 0.005\ \Omega$, $C = 0.052\ \Omega$, $\Delta = -0.025\ \Omega$, $g = 0.087\ \Omega$, $\gamma = 0.134\ \Omega$. The two bands braid around each other twice with a left handedness, as shown with the experimental measurements in Fig. 4a,c, giving rise to a braid degree $\nu = -2$ and a Hopf link. Then, by keeping all parameters the same as above but choosing $m = 3$, and also flipping the sign of Δ (that is, $\Delta = 0.025\ \Omega$), we can experimentally create two bands that braid three times with a braid degree $\nu = 3$, forming a trefoil (Fig. 4b,d). In general, more complex braids can be achieved with the use of larger m that results in a longer range coupling along the sublattice a in the Hamiltonian of equation (1) (further experimental results are provided in the Supplementary Information, section 3).

The braid group topology that we demonstrate for the bulk system has direct consequences manifested in the corresponding edge state spectrum. To illustrate this, we provide a detailed calculation of the edge-state spectrum for our two-band model in the Supplementary Information, section 1C. For a semi-infinite system, we show that for a braid degree $|\nu| > 0$, there is always a region in the energy space where the number of localized states is equal to $|\nu|$, and moreover, this region always contains an exceptional point of the energy spectrum. For a large finite lattice truncated by open boundary conditions, if the Bloch bands form a non-trivial braid with $|\nu| > 0$, the spectrum of such a finite lattice forms branches (Supplementary Fig. 6), and the number of branches is equal to the braid degree $|\nu|$. Although the results here are for our specific models, we believe that these observations can be proven more generally using the mathematical tools previously developed for studying the edge-state behaviours of systems exhibiting non-trivial point-gap topology[37,38,41].

To summarize, we have experimentally demonstrated non-trivial braids of two non-Hermitian bands in their complex band energies, as characterized by the braid group $\mathbb{B}_2$. By adding more resonators[29,30] or using extra degrees of freedom[33,42], such an experimental scheme can be used to achieve $\mathbb{B}_N$ group for $N > 2$, which should exhibit an even richer set of topological behaviours since $\mathbb{B}_N$ group becomes

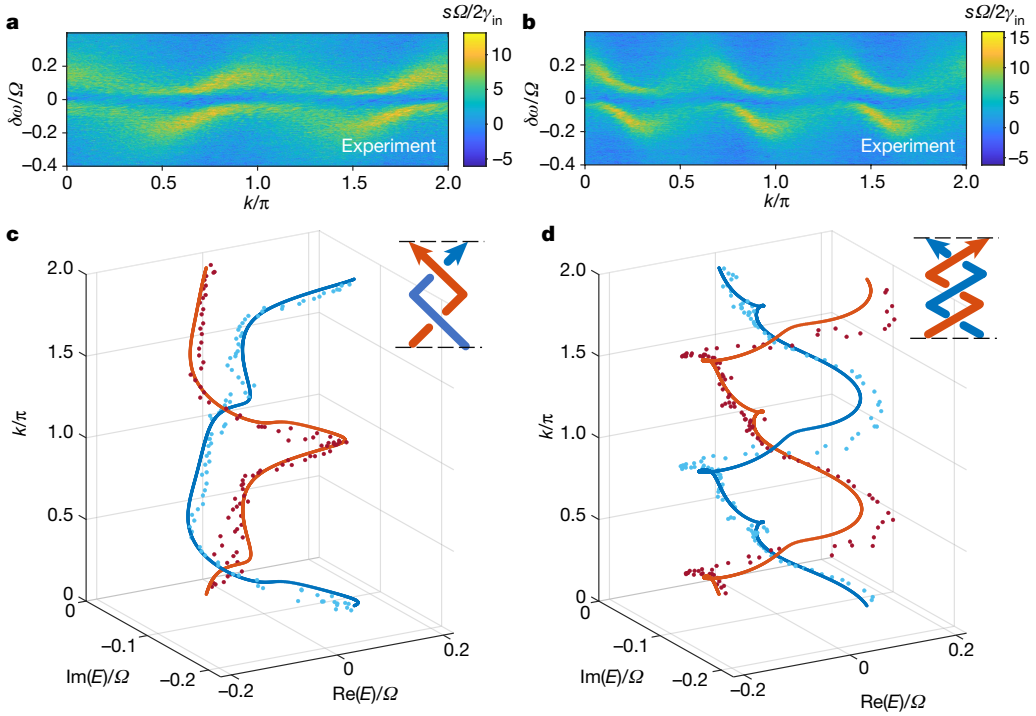

Fig. 4 | Complex-energy braids that form non-trivial links and knots. **a**,**b**, Experimentally measured signal $s(k, \delta\omega)$ for lattices with $m = 2$ (**a**) and $m = 3$ (**b**), with certain choices of parameters. **c**,**d**, Extracted complex-energy braiding using the measurement results in **a**,**b**, respectively. Dots denote experimental data and curves are theoretical predictions. Each braiding plot is accompanied by its corresponding braid diagram.

non-Abelian for $N > 2$ (for a specific discussion, see the Supplementary Information, section 4). The lattice we implement in synthetic frequency space can be truncated to introduce boundaries by incorporating extra ring resonators with a larger free spectral range[43]. Such a modified platform can be used to explore boundary effects in combination with complex-frequency excitation approaches such as virtual excitation[44]. We anticipate that our demonstration of braid-group non-Hermitian topology can open a pathway to the design and synthesis of a broad range of robust non-conservative systems exploiting the rich topological features associated with knot invariants.

Online content

Any methods, additional references, Nature Research reporting summaries, source data, extended data, supplementary information, acknowledgements, peer review information; details of author contributions and competing interests; and statements of data and code availability are available at https://doi.org/10.1038/s41586-021-03848-x.

1. Atiyah, M. *The Geometry and Physics of Knots* (Cambridge Univ. Press, 1990).
2. Leach, J., Dennis, M. R., Courtial, J. & Padgett, M. J. Knotted threads of darkness. *Nature* **432**, 165–165 (2004).
3. Kedia, H., Bialynicki-Birula, I., Peralta-Salas, D. & Irvine, W. T. M. Tying knots in light fields. *Phys. Rev. Lett.* **111**, 150404 (2013).
4. Shimokawa, K., Ishihara, K., Grainge, I., Sherratt, D. J. & Vazquez, M. FtsK-dependent XerCDdif recombination unlinks replication catenanes in a stepwise manner. *Proc. Natl Acad. Sci. USA* **110**, 20906–20911 (2013).
5. Wojcik, C. C., Sun, X.-Q., Bzdušek, T. & Fan, S. Homotopy characterization of non-Hermitian Hamiltonians. *Phys. Rev. B* **101**, 205417 (2020).
6. Lustig, E. et al. Photonic topological insulator in synthetic dimensions. *Nature* **567**, 356–360 (2019).
7. Yuan, L., Lin, Q., Xiao, M. & Fan, S. Synthetic dimension in photonics. *Optica* **5**, 1396–1405 (2018).
8. Adams, C. *The Knot Book* (American Mathematical Society, 2004).
9. Thomson, W. II. On vortex atoms. *London Edinburgh Phil. Mag. J. Sci.* **34**, 15–24 (1867).
10. Pisanty, E. et al. Knotting fractional-order knots with the polarization state of light. *Nat. Photon.* **13**, 569–574 (2019).
11. Pisanty, E. et al. Conservation of torus-knot angular momentum in high-order harmonic generation. *Phys. Rev. Lett.* **122**, 203201 (2019).
12. Lian, B., Vafa, C., Vafa, F. & Zhang, S. -C. Chern-Simons theory and Wilson loops in the Brillouin zone. *Phys. Rev. B* **95**, 094512 (2017).
13. Sun, X.-Q., Lian, B. & Zhang, S. -C. Double helix nodal line superconductor. *Phys. Rev. Lett.* **119**, 147001 (2017).
14. Wu, Q., Soluyanov, A. A. & Bzdušek, T. Non-Abelian band topology in noninteracting metals. *Science* **365**, 1273–1277 (2019).
15. Lee, C. H. et al. Imaging nodal knots in momentum space through topolectrical circuits. *Nat. Commun.* **11**, 4385 (2020).
16. Witten, E. Quantum field theory and the Jones polynomial. *Commun. Math. Phys.* **121**, 351–399 (1989).
17. Hu, H. & Zhao, E. Knots and non-Hermitian Bloch bands. *Phys. Rev. Lett.* **126**, 010401 (2021).
18. Weimann, S. et al. Topologically protected bound states in photonic parity–time-symmetric crystals. *Nat. Mater.* **16**, 433–438 (2017).
19. Bandres, M. A. et al. Topological insulator laser: experiments. *Science* **359**, eaar4005 (2018).
20. Zhou, H. et al. Observation of bulk Fermi arc and polarization half charge from paired exceptional points. *Science* **359**, 1009–1012 (2018).
21. Zhao, H. et al. Non-Hermitian topological light steering. *Science* **365**, 1163–1166 (2019).
22. Weidemann, S. et al. Topological funneling of light. *Science* **368**, 311–314 (2020).
23. Wang, K. et al. Generating arbitrary topological windings of a non-Hermitian band. *Science* **371**, 1240–1245 (2021).
24. Kozii, V. & Fu, L. Non-Hermitian topological theory of finite-lifetime quasiparticles: prediction of bulk Fermi arc due to exceptional point. Preprint at https://arxiv.org/abs/1708.05841 (2017).
25. Gao, T. et al. Observation of non-Hermitian degeneracies in a chaotic exciton-polariton billiard. *Nature* **526**, 554–558 (2015).
26. Li, Z. & Mong, R. S. K. Homotopical characterization of non-Hermitian band structures. *Phys. Rev. B* **103**, 155129 (2021).
27. Boada, O., Celi, A., Latorre, J. I. & Lewenstein, M. Quantum simulation of an extra dimension. *Phys. Rev. Lett.* **108**, 133001 (2012).
28. Ozawa, T. & Price, H. M. Topological quantum matter in synthetic dimensions. *Nat. Rev. Phys.* **1**, 349–357 (2019).
29. Yuan, L., Shi, Y. & Fan, S. Photonic gauge potential in a system with a synthetic frequency dimension. *Opt. Lett.* **41**, 741–744 (2016).
30. Ozawa, T., Price, H. M., Goldman, N., Zilberberg, O. & Carusotto, I. Synthetic dimensions in integrated photonics: from optical isolation to four-dimensional quantum Hall physics. *Phys. Rev. A* **93**, 043827 (2016).
31. Bell, B. A. et al. Spectral photonic lattices with complex long-range coupling. *Optica* **4**, 1433–1436 (2017).
32. Dutt, A. et al. Experimental band structure spectroscopy along a synthetic dimension. *Nat. Commun.* **10**, 3122 (2019).
33. Dutt, A. et al. A single photonic cavity with two independent physical synthetic dimensions. *Science* **367**, 59–64 (2020).
34. Wang, K. et al. Multidimensional synthetic chiral-tube lattices via nonlinear frequency conversion. *Light Sci. Appl.* **9**, 132 (2020).
35. Hu, Y., Reimer, C., Shams-Ansari, A., Zhang, M. & Loncar, M. Realization of high-dimensional frequency crystals in electro-optic microcombs. *Optica* **7**, 1189–1194 (2020).

36. Li, G. et al. Dynamic band structure measurement in the synthetic space. *Sci. Adv.* **7**, eabe4335 (2021).
37. Kawabata, K., Shiozaki, K., Ueda, M. & Sato, M. Symmetry and topology in non-Hermitian physics. *Phys. Rev.* **9**, 041015 (2019).
38. Gong, Z. et al. Topological phases of non-Hermitian systems. *Phys. Rev.* **8**, 031079 (2018).
39. Lee, T. E. Anomalous edge state in a non-Hermitian lattice. *Phys. Rev. Lett.* **116**, 133903 (2016).
40. Shen, H., Zhen, B. & Fu, L. Topological band theory for non-Hermitian Hamiltonians. *Phys. Rev. Lett.* **120**, 146402 (2018).
41. Okuma, N., Kawabata, K., Shiozaki, K. & Sato, M. Topological origin of non-Hermitian skin effects. *Phys. Rev. Lett.* **124**, 086801 (2020).
42. Yuan, L. et al. Photonic gauge potential in one cavity with synthetic frequency and orbital angular momentum dimensions. *Phys. Rev. Lett.* **122**, 083903 (2019).
43. Buddhiraju, S., Dutt, A., Minkov, M., Williamson, I. A. D. & Fan, S. Arbitrary linear transformations for photons in the frequency synthetic dimension. *Nat. Commun.* **12**, 2401 (2021).
44. Baranov, D. G., Krasnok, A. & Alù, A. Coherent virtual absorption based on complex zero excitation for ideal light capturing. *Optica* **4**, 1457–1461 (2017).

Methods

Implementation of non-Hermitian lattice Hamiltonians in frequency synthetic space

The experimental setup in Fig. 2a implements the Hamiltonian of equation (1). The operators $\mathbf{a}_n^\dagger$ ($\mathbf{a}_n$) and $\mathbf{b}_n^\dagger$ ($\mathbf{b}_n$) in equation (1) correspond to the creation (annihilation) of the n-th frequency mode ($\omega_n = \omega_0 + n\Omega$) in resonator a and b, respectively. We utilize a pair of modes in the two rings propagating along opposite directions (Fig. 2a). The coupling of modes at the same frequency between the two resonators implements the terms $g\ \mathbf{a}_n^\dagger\mathbf{b}_n + g\ \mathbf{b}_n^\dagger\mathbf{a}_n$ in equation (1). The loss difference γ between the two sublattices is realized by adding an additional loss rate γ in resonator a for all frequencies. In practice, as resonator a contains modulators, whereas resonator b does not, the loss rates of the two resonators are usually different. The couplings between the frequency modes in resonator a are implemented via a dynamic modulation. Specifically, the Hermitian coupling terms $\kappa\mathbf{a}_{n+1}^\dagger\mathbf{a}_n + \kappa\mathbf{a}_n^\dagger\mathbf{a}_{n+1} + C\mathbf{a}_{n+m}^\dagger\mathbf{a}_n + C\mathbf{a}_n^\dagger\mathbf{a}_{n+m}$ are achieved by a phase modulator that generates a time-dependent transmission $T_{\mathrm{Ph}} = \exp[-iK\cos(\Omega t) - iA\cos(m\Omega t)]$, and we have $\kappa \propto K$ and $C \propto A$. The skew-Hermitian coupling terms $-\Delta\mathbf{a}_{n+m}^\dagger\mathbf{a}_n + \Delta\mathbf{a}_n^\dagger\mathbf{a}_{n+m}$ are achieved by an amplitude modulator with the time-dependent transmission $T_{Am} = 1 + B\sin(m\Omega t)$ that gives rise to $\Delta \propto B$. In both cases, the terms implemented by the modulation with frequency $m\Omega$, with m being an integer, introduce the long-range coupling when $m > 1$. As an example, the $m = 2$ case is shown (Fig. 2b, right; further information about such an implementation is provided in the Supplementary Information, section 1D).

Measurement of complex band structures

We measure the complex-energy band structure in the frequency synthetic space for the experimental system of Fig. 2a. Here, we briefly summarize the theory that underlies such a measurement. More details can be found in refs. [23,32] as well as in the Supplementary Information. In general, to measure the band structure $E(k)$ of any lattice system, one can measure a response function of the system as a function of E and k. The band structure then corresponds to the resonance in such a response function. Since our lattice space is along the frequency axis, its reciprocal space is the time (t) axis, and we can define a quasi-momentum along the frequency axis, $k = t\Omega$. As our system is modulated periodically in time, with the modulation period equal to the free spectral range, its 'energy' is inherently the Floquet quasi-energy, corresponding to the detuning $\delta\omega$ of the excitation frequency off any resonant frequency ω_n (Fig. 2b, right). Therefore, we excite the system with a tunable continuous-wave laser, and we measure the system as we sweep the frequency of the laser across a resonant frequency ω_n. At each specific detuning $\delta\omega$, we allow the system to reach the steady state, and then perform a measurement of its transmission coefficient (see Fig. 2a) as a function of time. The resulting time-dependent transmission coefficient can be written as

$$s(k, \delta\omega) = 1 - \langle a|\mathbf{S}_k^\dagger(\delta\omega)\mathbf{S}_k(\delta\omega)|a\rangle, \tag{5}$$

where the 2×2 matrix $\mathbf{S}_k = \mathbf{I}_2 + i\gamma_{\mathrm{in}}(\mathbf{H}_k - \delta\omega - i\gamma_{\mathrm{in}}/2)^{-1}$ with γ_{in} being the effective in–out coupling constant and $\mathbf{I}_2$ the 2×2 identity matrix. In equation (5), the first term '1' corresponds to the direct transmission of the incident wave without exciting any resonance. In the second term, $|a\rangle = [1, 0]^{\mathrm{T}}$ since we directly excite resonator a; moreover, a part of the transmission as described by this term is the leakage radiation of resonator a into the output waveguide. Assuming a small γ_{in}, we have

$$\begin{aligned} s(k, \delta\omega) &\approx 2\gamma_{\mathrm{in}}\mathrm{Im}[\langle a|(\mathbf{H}_k - \delta\omega)^{-1}|a\rangle] \\ &= 2\gamma_{\mathrm{in}}\mathrm{Im}\left[\mu_+(k)\frac{1}{E_+(k) - \delta\omega} + \mu_-(k)\frac{1}{E_-(k) - \delta\omega}\right], \end{aligned} \tag{6}$$

where the coefficients satisfy $\mu_+(k) + \mu_-(k) = 1$ and E_+, E_- denote the two eigenvalues of $\mathbf{H}_k$. At each $\delta\omega$, we perform a fitting of the measured $s(k, \delta\omega)$ as a function of k using equation (6) to extract the values of E_+ and E_- in both real and imaginary parts (see Supplementary Information, section 2B, for further details).

We emphasize that our measurement approach allows us to determine the band structure that corresponds to an infinite periodic system as long as our lattice in the experiment possesses a sufficient number of lattice sites[23], without the need for periodic boundary conditions. It is known that for non-Hermitian Hamiltonians, the eigenstates of a finite system can be drastically different from those of an infinite periodic system even if there are a large number of lattice sites. Nevertheless, here our measurement is not an observation of the eigenvalues of the finite system. Instead, the t-resolved detection projects the Hamiltonian to the space spanned by the state $|k_a\rangle = |a\rangle \otimes |k\rangle$ to obtain the expectation value $\langle k_a|\mathbf{H}|k_a\rangle$, where the discrete Bloch state $|k_a\rangle$ of sublattice a is always extended. The measurement outcome thus naturally approaches the corresponding quantities in the infinite periodic system as the number of lattice sites increases.

Data availability

The data that support the findings of this study are available in Figshare at https://doi.org/10.6084/m9.figshare.14925087.

Code availability

The code that supports the findings of this study is available in Figshare at https://doi.org/10.6084/m9.figshare.14925087.

Acknowledgements We thank D. A. B. Miller for providing laboratory space and equipment and X.-Q. Sun for discussions. This work is supported by a MURI project from the US Air Force Office of Scientific Research (grant no. FA9550-18-1-0379), and by a Vannevar Bush Faculty Fellowship from the US Department of Defense (grant no. N00014-17-1-3030).

Author contributions K.W., C.C.W. and S.F. conceived the study; K.W. and C.C.W. developed the theory and performed numerical simulations; K.W. and A.D. performed the experiments and processed experimental data. All authors discussed the results and contributed to writing the manuscript. S.F. supervised the work.

Competing interests The authors declare no competing interests.

Additional information
Supplementary information The online version contains supplementary material available at https://doi.org/10.1038/s41586-021-03848-x.
Correspondence and requests for materials should be addressed to S.F.
Peer review information *Nature* thanks Biao Yang and the other, anonymous, reviewer(s) for their contribution to the peer review of this work.